**Article:**
Bou-Francis, A, Soyka, RPW, Ferguson, SJ et al. (2 more authors) (2015) Novel methodology for assessing biomaterial-biofluid interaction in cancellous bone. Journal of the Mechanical Behavior of Biomedical Materials, 46. pp. 158-167. ISSN 1751-6161

https://doi.org/10.1016/j.jmbbm.2015.02.027

## 1.0 Introduction

Osteoporosis and other skeletal pathologies such as spinal metastasis and multiple myeloma, compromise the structural integrity of the vertebra, thus increasing its fragility and susceptibility to fracture [1-3]. During vertebral augmentation procedures, bone cement is injected through a cannula into the cancellous bone of a fractured vertebra with the goal of relieving pain and restoring mechanical stability. Further, prophylactic surgical stabilization is often performed to reinforce a structurally compromised vertebra adjacent to the index level and decrease its susceptibility to fracture [4, 5]. The bone cements used are chemically complex, multi-component and non-Newtonian with their viscosity having differing degrees of time and shear rate dependency. These cements interact with the porous structures though which they flow and with other fluids present within the porous media. The most widely used cement, poly(methyl methacrylate) (PMMA), is generally assumed insoluble in any biofluid (bone marrow) it comes into contact with, thus the cement-marrow displacement is characterized as a two-phase immiscible flow in porous media [6, 7]. As vertebral cancellous bone displays highly complex geometrical structures and architectural inhomogeneities over a range of length scales, the pore-scale cement viscosity varies due to its non-linear dependency on shear rates, which are affected by variations in the local tissue morphology. Furthermore, the vertebral cancellous bone microarchitecture varies among the patients being treated, thus making the scientific understanding of the cement flow behaviour difficult in clinical or, indeed, cadaveric studies [8, 9]. Previous experimental studies on cement flow [8, 11-14] have used open-porous aluminum foam to represent osteoporotic bone. Although the porosity was well controlled, the geometrical structure of each of the foams was inherently unique. This paper presents novel methodology using customised, reproducible and pathologically representative three-dimensional bone surrogates to help study biomaterial-biofluid interaction. The aim is to provide a clinical representation of cement flow distribution and a tool for validating computational simulations.

## 2.0 Materials and methods

### 2.1 Bone Surrogate Development

Three-dimensional bone surrogates were developed to mimic the human vertebral body (Figure 1). The surrogates were designed in SolidWorks (Dassault Systèmes, Vélizy, France) then manufactured using a rapid prototyping technique (Projet HD 3000, 3D Systems, Rock

Hill, South Carolina, USA). The structure of the surrogates was tailored to mimic three skeletal pathologies: osteoporosis (Osteo), spinal metastasis (Lesion) and multiple myeloma (MM). Figure 2 illustrates the developed bone surrogates and Table 1 describes the elements incorporated into each surrogate. Once the surrogates were manufactured, microCT (µCT 100, Scanco Medical, Switzerland) was used to assess the variability in their morphology. Eight of the Osteo surrogates were scanned at a spatial resolution of 24.6 µm (isotropic voxel size). Then, a cylindrical volume of interest 15 mm in diameter and 15 mm in length was consistently defined at the centre of each specimen. Within this volume of interest, a threshold of -120 HA mg/ccm (based on Ridler's method [15]) was applied and the three-dimensional morphometric indices were determined using proprietary software (Scanco Medical, Switzerland). Only the bone volume fraction, BV/TV (%), trabecular thickness, Tb.Th (mm), and trabecular separation, Tb.Sp (mm) were compared. The porosity of the specimens was obtained from the micro-CT data (100 - BV/TV) and validated using Archimedes' suspension method of measuring volume [16] which was performed using six cubes ($2 \times 2 \times 2$ $cm^3$) with the same structure as the Osteo surrogates. One of the six cubes was also used to measure the permeability of the Osteo structure using Darcy's law [17, 18]. Furthermore, static contact angle analysis (FTA 4000, First Ten Angstroms, Virginia, USA) was performed on the material to compare the surface wettability to that of cortical bone from a dry human femur and a fresh ovine vertebra.

## 2.2 Experimental Protocol

The surrogates were filled with bone marrow substitute prepared using an aqueous solution of 2.5% w/w carboxymethyl cellulose ($M_w$ ~250,000 - Sodium carboxymethyl cellulose, Sigma-Aldrich, Missouri, USA) with a nominal viscosity of 0.4 Pa·s which has been reported as the approximate value for red bovine marrow [19]. Superior and inferior plates were used to create a tight seal and confine the marrow within the surrogates. Following this, the surrogates were placed into the experimental set-up (Figure 3) and Simplex P bone cement (Stryker Corporation, Michigan, USA) was injected into each bone surrogate under a constant flow rate of 3 mL/min. A modified formulation for Simplex P was prepared using 10 mL liquid monomer, 9 g PMMA powder and 1 g $BaSO_4$. The cement was mixed [20] then transferred into a 10 mL syringe and injected at 4 and 8 min from mixing (SP4 and SP8, respectively) to assess the effect on the flow behaviour. The same syringe, needle and cement

were used to perform the two injection time points into separate surrogates. The flow behaviour was tested in each structure, and all injections were repeated three times.

The injections were performed using a 10 mL luer-lok syringe (Becton Dickinson, New Jersey, USA) with a 12-gauge needle (Blunt SS 12-gauge × 4 inch, W. W. Grainger Inc, Illinois, USA). All injections were performed at room temperature (21.5 ± 0.1 ºC) using a unilateral approach. The needles were consistently placed through the left insertion channel, while the entry point on the outside of the right insertion channel remained closed off to prevent any fluid from escaping through the cortex. A fluoroscope (BV-25, Philips, Eindhoven, Netherlands) was used to radiographically monitor the injections, while a specimen holder was designed to keep the surrogates at the same height with respect to the fluoroscope. Further, the holder ensured that the top plane of the surrogates was parallel to the plane of the fluoroscope.

## 2.3 Data Analysis

The displacement of the syringe plunger and the force applied on the plunger were used to determine the injection flow rate and pressure, respectively. The measured force was divided by the cross-sectional area of the syringe to determine the total pressure in the system, which is the sum of two pressures: 1) $\Delta P_n$, the pressure required to overcome frictional forces and to inject the fluid through the needle and 2) $\Delta P_s$, the pressure required to inject the fluid into the structure of the bone surrogates. For this reason, injections were also performed without the surrogates to determine $\Delta P_n$, which was then subtracted from the total pressure to determine $\Delta P_s$ at the inlet.

The video sequences showing the superior view of the fluoroscopy projection were analyzed in Matlab (R2009b, MathWorks, Massachusetts, USA). This allowed automated segmentation of the flow contours by subtracting the first frame of the video sequence, which shows the surrogates with no fluid injected, from the remaining frames. The error in the needle placement within the surrogates was quantified on the first video frame through measuring the needle length and angle with respect to the posterior wall. The mean spreading distance (MSD) was measured on the segmented flow contours. The shortest and longest distances were determined along the geometric center of each contour and MSD was calculated by taking the mean of the two distances. Furthermore, the time and type of leakage (i.e. anterior or posterior) were obtained directly from the video sequences.

The construct was scanned using microCT post-injection at a spatial resolution of 73.6 µm (isotropic voxel size). The DICOM stack of each scan was processed in imageJ [21] to obtain the final shape of the cement bolus and measure the sphericity (Eq. 1), which is defined as the surface area of a sphere enclosing the same volume (V) as the 3D object, divided by the surface area (A) of the structure [22].

$$\text{Sphericity} = \frac{\sqrt[3]{36\pi V^2}}{A} \qquad (1)$$

All data were presented as mean ± standard deviation. The influence of the viscosity and the structure on the measured parameters was evaluated using the Mann–Whitney U and the Kruskal-Wallis one-way analysis of variance with a significance level set at $\alpha = 0.05$. All statistical analyses were performed in SPSS version 21 (SPSS Inc, Illinois, USA).

## 2.4 Experimental/Computational Cross-validation

The developed CAD model of each bone surrogate was converted into a continuum scale finite element model similar to that previously utilised for assessing cement flow in bone [9]. The computer simulation was set up with the same boundary conditions as the experiments. Then, the flow behaviour of Simplex P bone cement was simulated in each bone surrogate for an injected volume of 5 mL at a constant flow rate of 3 mL/min matching that undertaken in the experiments. The marrow substitute was modeled in the simulation using viscosity measurements performed using a rheometer (Malvern Instruments Ltd, Malvern, UK) in rotation mode with a cone on plate configuration. The cone had a 25 mm radius and 1º angle. The temperature was set to 21ºC and the angular speed of the cone (Ω) was ramped to achieve varying shear rates from 0 to 100 $s^{-1}$. The ramp time was 5 min and 10 samples per decade were recorded. The Simplex P formulation was modeled in the simulation for injections performed at 4 min after cement mixing (SP4). The viscosity was based on previously published rheological tests [9].

# 3.0 Results

## 3.1 Viscosity Measurements

The rheological tests revealed that the marrow substitute had a viscosity of approximately 0.39 Pa·s for shear rates ranging from 1 to 100 $s^{-1}$ and exhibited Newtonian fluid characteristics (viscosity independence to shear rate).

## 3.2 Bone Surrogate Characterization

The variability in the morphology of the Osteo surrogates was very low with an overall strut thickness (Tb.Th) of 0.25 ± 0.04 mm and pore spacing (Tb.Sp) of 0.89 ± 0.03 mm. The histogram of the thickness map revealed two distinct peaks at approximately 0.18 and 0.27 mm corresponding to the horizontal and vertical struts of the 3D bone surrogates, which had a nominal thickness of 0.15 and 0.25 mm, respectively. The mean porosity, which was obtained from the microCT data, was 82.6 ± 1.1 %. The measured permeability of the Osteo structure was 57.1 ± 6.1 × $10^{-10}$ $m^2$. The surface wettability was comparable between materials with contact angles ranging from 49 to 77º for the substance used to manufacture the bone surrogates, 60 to 75º for bone from a dry human femur and 58 to 69º for bone from a fresh ovine vertebra.

## 3.3 Injection Parameters

The measured displacement of the syringe plunger confirmed the injection flow rate to be constant at 2.99 ± 0.01 mL/min. Multiplying the total displacement of the syringe plunger by the cross-sectional area of the syringe confirmed that the injected volume was 4.95 ± 0.01 mL. The mean needle length from the posterior wall was 23 ± 1 mm and the mean needle angle with respect to the posterior wall was 70 ± 2º. As the nominal CAD distance is 25 mm and the nominal CAD angle is 69.8º, the mean error was 8% for the needle length (d) and 0.1% for the needle angle.

## 3.4 Flow Distribution

In the Osteo surrogate, the experiments showed that cement injected at 4 min (SP4) had a tendency to flow laterally into the right needle insertion channel (Figure 4). This behaviour was not observed in the MM and Lesion surrogates, independent of the cement injection time, mainly due to the flow being guided by the lesions. The flow distribution obtained numerically via the computer simulation was similar to that observed experimentally in the Osteo and MM surrogates, although the simulation predicted lateral flow in the MM surrogate which was not observed experimentally. In the Lesion surrogate, the simulated flow

was towards the anterior boundary and along the right needle insertion channel, while the experimental flow was channelled by the void towards the posterior wall.

Qualitative analysis of the experimental data also showed that in the Osteo and MM surrogates there was a high tendency for anterior leakage only, because the cements never reached the posterior wall. In the Lesion surrogate, there was a high tendency for posterior leakage only, although the cement injected at 8 min (SP8) reached the anterior wall. The computer simulation predicted anterior leakage in all the bone surrogates, thus matching the experiments in the Osteo and MM surrogates only.

## 3.5 Sphericity

Increasing the injection time from 4 to 8 min after cement mixing significantly increased ($p < 0.05$) the sphericity by 12.6% in the Lesion surrogate only (Table 2 and Figure 5). Furthermore, introducing structural voids significantly ($p < 0.05$) decreased the sphericity of the SP4 cement only. Relative to the Osteo surrogate, the presence of the large void in the Lesion surrogate caused a more pronounced decrease (11.0%) in sphericity compared to the presence of three small voids in the MM surrogate (7.7%). The sphericity obtained numerically for the SP4 cement was similar to that measured experimentally in the Osteo surrogate (5.9% difference). In the MM surrogate, the sphericity obtained numerically was 14.9% higher than that measured experimentally, although the simulated flow distribution was qualitatively similar. In the Lesion surrogate, the difference in the sphericity obtained numerically and that measured experimentally was less pronounced (10%), which is interesting especially when the simulated flow was preferentially horizontal towards the anterior boundary while the experimental flow was along the posterior void.

## 3.6 Mean Spreading Distance (MSD)

Increasing the cement injection time did not have a significant ($p = 0.321$) effect on the MSD, independent of the structure (Table 2). Similarly, introducing structural voids did not have a significant ($p = 0.104$) effect on the MSD, independent of the cement injection time. The MSD obtained numerically was overestimated by 22.7%, 16.3% and 34.2% in the Osteo, MM and Lesion surrogates, respectively.

### 3.7 Leakage Time

The experimental results showed that increasing the cement injection time significantly ($p < 0.05$) increased the leakage time in the Osteo surrogate by 39.1% and in the MM surrogate by 49.4% (Table 2). The leakage time in the Lesion surrogate remained the same independent of the cement injection time. For SP4 cement only, the structural void in the Lesion surrogate caused a significant ($p < 0.05$) increase (95.3%) in the leakage time, relative to the Osteo surrogate. Figure 6 presents typical leakage observed in the Osteo and Lesion surrogates.

### 3.8 Injection Pressure

The experimental results also showed that increasing the cement injection time significantly ($p < 0.05$) increased the peak pressure by 183.0% in the Osteo surrogate, 54.2% in the MM surrogate and 133.7% in the Lesion surrogate (Table 2 and Figure 7). Furthermore, the presence of structural voids generally decreased the peak pressure independent of the cement injection time. For the SP4 cement, the peak pressure recorded in the MM surrogate was similar to that recorded in the Osteo surrogate (7.6% difference). However, the structural void in the Lesion surrogate decreased the peak injection pressure by 29.5% relative to the Osteo surrogate. For the SP8 cement, the structural voids in the MM and Lesion surrogates decreased the peak injection pressure by 41.4% relative to the Osteo surrogate.

## 4.0 Discussion

The developed bone surrogates can be assumed constant in terms of their geometrical structure as the variability in morphology was very low. This is crucial to reduce the inconsistency, render the experiments reproducible and shift the focus onto understanding the influence of viscosity and structure on the flow behaviour. The pore spacing of the Osteo surrogates ($0.89 \pm 0.03$ mm) was comparable to that reported in the literature for human osteoporotic vertebral cancellous bone [23-27], suggesting that the surrogates were pathologically representative. The boundary of the surrogates simulated the vertebral shell which confines the flow and controls the intravertebral pressure, significantly affecting the filling pattern [28]. This is consistent with previous studies in which Loeffel et al. [13] sealed their surrogates with a reusable acrylic enclosure, while Baroud et al. [11] and Mohamed et al. [14] coated their surrogates with a 1 mm layer of acrylic cement to mimic the vertebral shell. The boundary including the inlet and the flow exit points were kept constant for all the

surrogates within this study. The openings in the boundary simulate breaches through the cortex due to a lesion and/or a vessel exchanging blood in and out of the vertebral body. This is important as such breaches create paths of least resistance providing means for leakage into the surrounding structures. Furthermore, the proposed surrogates simulate the rheological environment within the vertebral body. The measured permeability of the Osteo surrogates ($57.1 \pm 6.1 \times 10^{-10}$ $m^2$) was comparable to that reported by Nauman et al. [29] for human vertebral cancellous bone. Also, the surface wettability of the surrogates matches that of bone and the presence of the marrow substitute simulates the two-phase flow that occurs within the vertebral body. In previous studies, Bohner et al. [8] and Loeffel et al. [13] both used melted cow butter, whereas Baroud et al. [11] and Mohamed et al. [14] both used a water/gelatin solution. A true representation of the rheological properties of human red bone marrow present within the cancellous bone is extremely important as such properties significantly affect the cement flow behaviour [8].

In all the experiments, the flow rate was kept constant at 3 mL/min and maintained for the duration of the injection. The chosen flow rate was similar to that reported in previous cadaveric studies [30, 31] and falls within the range reported during clinical percutaneous vertebroplasty (PV) which is 1.2 to 12.0 mL/min [32]. However, in clinical PV intermittent injections are typically performed with pauses due to changing of syringes and/or the needle position, which is often retracted backwards due to excessive pressurization [32]. The continuous injection was necessary to simplify the injection parameters.

Loeffel et al. [13] were the only group to study the influence of viscosity on the cement spreading pattern in human cadaveric vertebrae as well as foam material with similar morphological properties. Their results showed that the measured circularity, which was used to quantitatively describe the final shape of the cement bolus, was similar in the cadaveric samples as well as the foam material, suggesting that bone surrogates can be used to achieve a clinical representation of cement flow distribution. Loeffel et al. [13] also found that increasing the cement viscosity from 50 to 100 Pa·s, resulted in significantly denser and more circular cement patterns (higher circularity). In the current study however, all the viscosities tested were below 100 Pa·s [9] which may explain why increasing the cement starting viscosity did not have a significant ($p < 0.05$) effect on the MSD, independent of structure.

The leakage patterns observed in the Osteo surrogate were similar to those reported by Lador et al. [38] who studied the points and pattern of cement extravasation in 23 human vertebrae and showed that the most common type of leakage, classified as severe, was through small breaches in the cortex due to anterior blood vessels. This type of leakage

occurred in 83% of the samples, thus highlighting the importance of monitoring all vertebral walls for cement extravasation through breaches in the cortex to avoid complications and minimize possible life-threatening risks to the patients. This is mainly because leakage into the surrounding vasculature can reach remote areas of the body, such as the lungs, and cause pulmonary embolisms [39-41]. The posterior leakage typically observed in the Lesion surrogate was similar to that reported by Reidy et al. [31] who studied the cement filling pattern in seven osteoporotic human vertebrae with simulated lytic lesion. Their results showed that the cement leakage through the posterior venous foramen of the vertebra into the spinal canal occurred in 86% of the samples. This highlights the importance of monitoring cement extravasation through the posterior wall in patients with metastatic involvement to avoid complications such as nerve root or spinal cord compression [42]. It is interesting to note that the structural void in the current Lesion surrogate generally increased the leakage time under the chosen injection parameters. This is not surprising especially when posterior leakage occurred and the target site for cement deposition was at the anterior third. Also, the filled volume is large due to the presence of the structural void. Furthermore, the leakage time in the Osteo and MM surrogates increased with the cement injection time. This is consistent with the study by Baroud et al.[11] who also reported immediate leakage at the early injection time point of 5 min after cement mixing.

As expected, the injection pressure measured in this study significantly ($P < 0.05$) increased with an increase in the cement injection time. This is consistent with the study by Kerbs et al. [32] who also reported significantly ($P < 0.001$) higher in vivo cement injection pressure during the later phase of the cement polymerization (7 vs. 11 min from mixing). Furthermore, the presence of structural voids generally decreased the peak injection pressure independent of the cement injection time. This is not consistent with the study by Reidy et al. [31] who reported no significant difference in the force required to inject bone cement into osteoporotic human vertebrae with and without simulated lytic lesion. In their study however, the lesion was filled with soft tumour tissue. It is important to note that the overall flow resistance of the vertebra is mainly a function of the cortical shell, the porosity and the rheological properties of the “fluid” phases (tumour and/or marrow) present within the trabecular network [31]. From a geometrical perspective only, the presence of lytic lesion increases the porosity thus the hydraulic permeability and the overall flow resistance of the vertebra, which decreases the peak injection pressure as evident in the results of this study. On the other hand, soft tumour tissue (with higher viscosity relative to bone marrow) present within the lesion decreases the overall flow resistance of the vertebra. This may explain why

there was no significant difference in the force reported by Reidy et al. [31] required to inject bone cement into osteoporotic human vertebrae with and without simulated lytic lesion. Further experiments are required to elucidate the effects of soft tumour tissue on the injection biomechanics.

This study demonstrates that the computational model developed to simulate the flow of two immiscible fluids through porous media [9] generally agrees with the experimental data in the Osteo and MM surrogates. The difference between the experimental data and the simulations was more pronounced in the Lesion surrogate. The computational flow model is based on the assumption that the flow process of two immiscible fluids is mainly governed by the structural properties of the porous medium and the rheological properties of the fluids present within the porous medium. Thus, the accuracy of the simulation depends inherently on how the permeability coefficients are determined and how the viscosities of the two fluids are measured. In the current simulation [9], the permeability was estimated using the Kozeny equation which is based on hydraulic radius theories. The assumptions of such theories hold well in the Osteo surrogate and may explain the strong agreement between the simulations and the experimental data. In the Lesion and MM surrogates, the voids were modelled as high-permeable regions. Moreover, the equations hold on average in these surrogates and may explain the weaker agreement. A further source of error for the discrepancy in the Lesion surrogate may be due to the difference between the experimental needle tip position and the nominal position of the injection inlet in the CAD model, which was adopted in the simulation. The needle length from the posterior wall measured experimentally on the superior view of the fluoroscopy projection was on average 2 mm shorter (i.e. closer to the posterior wall) compared to nominal position of the inlet in the simulations. This could have a significant effect on the flow behavior and may explain the difference between the simulated and the experimental flow patterns. Additional experiments are needed to clarify the effect of needle tip position, especially in the presence of a large structural void.

In the current simulation, the viscosities of the fluid phases were governed using a power law, which adjusts the viscosity of each fluid phase depending on the time and the shearing rate [9]. Although the viscosities were characterized with respect to time and shear rate, the accuracy of the simulation is inherently dependent on how the shear rate is determined. In this simulation, the shear rate was computed from the Darcy flux and empirically related to the microscopic length scale [9]. Furthermore, the simulation neglects other factors that may affect the rheology of the fluids such as the fluid temperature or the yield stresses. More importantly, the simulation expresses Darcy's law in the form of one single constitutive

equation in terms of the mixture of both fluid phases and does not take into account the potential effect of the fluid-fluid interface induced by the surface tension. However, this study shows that computer simulation can be used to predict the cement placement in cancellous bone, which has been identified as a critical parameter in the biomechanical behaviour of the construct post-augmentation [43, 44].

The advantage of the experimental methodology presented here, is that it provides a clinically relevant representation of cement flow patterns and a tool for validating computational simulations. The design of the experimental set-up facilitates the modeling aspect of the simulation. The injection parameters (i.e. needle gauge, needle placement, flow rate and injected volume) were well controlled and reproducible for all the injections. The boundary including the openings and the needle insertion channels were kept constant for all surrogates. Furthermore, the structure of the surrogates was uniform to reduce the variability in the morphology (i.e. thickness and spacing) and the structural geometry, thus achieving a near constant intrinsic permeability coefficient, particularly in the Osteo surrogate. It is important to control the structural properties as these dictate the permeability tensor and in combination with the applied pressure gradient the flow in the porous medium.

## 5.0 Conclusion

This paper presents novel methodology using reproducible and pathologically representative three-dimensional bone surrogates to help study biomaterial-biofluid interaction providing a clinical representation of cement flow distribution and a tool for validating computational simulations. The proposed bone surrogates overcome the limitations of previous materials as their geometrical structure is well controlled and can be tailored to mimic the morphology of specific bone conditions at different skeletal sites. This allows for the pathological representation to remain fixed between investigations and the effects of subtle differences in the injection behaviour to be assessed in a reproducible manner.

## 6.0 Funding

This work was funded by the European Union under the FP7 Marie Curie Action, grant agreement no. PITN-GA-2009-238690-SPINEFX.

## References


1. Bouxsein, M.L., Bone quality: where do we go from here? Osteoporos Int, 2003. **14 Suppl 5**: p. S118-27.
2. Currey, J.D., Bone strength: what are we trying to measure? Calcif Tissue Int, 2001. **68**(4): p. 205-10.
3. Myers, E.R. and S.E. Wilson, Biomechanics of osteoporosis and vertebral fracture. Spine (Phila Pa 1976), 1997. **22**(24 Suppl): p. 25S-31S.
4. Ortiz, O. and J.M. Mathis, Vertebral body reconstruction: techniques and tools. Neuroimaging Clin N Am, 2010. **20**(2): p. 145-58.
5. Mathis, J.M. and W. Wong, Percutaneous vertebroplasty: technical considerations. J Vasc Interv Radiol, 2003. **14**(8): p. 953-60.
6. Pinder, G.F. and W.G. Gray, Essentials of Multiphase Flow and Transport in Porous Media. 2008: John Wiley & Sons, Inc.. .
7. Widmer, R.P. and S.J. Ferguson, A mixed boundary representation to simulate the displacement of a biofluid by a biomaterial in porous media. J Biomech Eng, 2011. **133**(5): p. 051007.
8. Bohner, M., et al., Theoretical and experimental model to describe the injection of a polymethylmethacrylate cement into a porous structure. Biomaterials, 2003. **24**(16): p. 2721-30.
9. Widmer Soyka, R.P., et al., Numerical description and experimental validation of a rheology model for non-Newtonian fluid flow in cancellous bone. J Mech Behav Biomed Mater, 2013. **27**: p. 43-53.
10. Widmer Soyka, R.P., et al., Numerical description and experimental validation of a rheology model for non-Newtonian fluid flow in cancellous bone. J Mech Behav Biomed Mater, 2013. **6161**(13): p. 00214-2.
11. Baroud, G., M. Crookshank, and M. Bohner, High-viscosity cement significantly enhances uniformity of cement filling in vertebroplasty: an experimental model and study on cement leakage. Spine (Phila Pa 1976), 2006. **31**(22): p. 2562-8.
12. Habib, M., et al., Cement leakage and filling pattern study of low viscous vertebroplastic versus high viscous confidence cement. The International Society for the Advancement of Spine Surgery, 2010. **4**: p. 26-33.
13. Loeffel, M., et al., Vertebroplasty: experimental characterization of polymethylmethacrylate bone cement spreading as a function of viscosity, bone porosity, and flow rate. Spine (Phila Pa 1976), 2008. **33**(12): p. 1352-9.
14. Mohamed, R., et al., Cement filling control and bone marrow removal in vertebral body augmentation by unipedicular aspiration technique: an experimental study using leakage model. Spine (Phila Pa 1976), 2010. **35**(3): p. 353-60.
15. Ridler, T.W. and S. Calvard, Picture Thresholding Using an Iterative Selection Method. Systems, Man and Cybernetics, IEEE Transactions on, 1978. **8**(8): p. 630-632.
16. Hughes, S.W., Archimedes revisited: a faster, better, cheaper method of accurately measuring the volume of small objects. Physcis Education, 2005. **40**(5).
17. Baroud, G., et al., Experimental and theoretical investigation of directional permeability of human vertebral cancellous bone for cement infiltration. J Biomech, 2004. **37**(2): p. 189-96.
18. Widmer, R.P. and S.J. Ferguson, On the interrelationship of permeability and structural parameters of vertebral trabecular bone: a parametric computational study. Comput Methods Biomech Biomed Engin, 2012. **16**(8): p. 908-22.

19. Bryant, J.D., et al., Rheology of bovine bone marrow. Proc Inst Mech Eng H, 1989. **203**(2): p. 71-5.
20. Bou-Francis, A., et al., Assessing cement injection behaviour in cancellous bone: An in vitro study using flow models. J Biomater Appl, 2014. **29**(4): p. 582-94.
21. Schneider, C.A., W.S. Rasband, and K.W. Eliceiri, NIH Image to ImageJ: 25 years of image analysis. Nat Meth, 2012. **9**(7): p. 671-675.
22. Lin, C.L. and J.D. Miller, 3D characterization and analysis of particle shape using X-ray microtomography (XMT). Powder Technology, 2005. **154**(1): p. 61-69.
23. Chen, H., et al., Regional variations of vertebral trabecular bone microstructure with age and gender. Osteoporos Int, 2008. **19**(10): p. 1473-83.
24. Gong, H., et al., Regional variations in microstructural properties of vertebral trabeculae with structural groups. Spine (Phila Pa 1976), 2006. **31**(1): p. 24-32.
25. Hildebrand, T., et al., Direct three-dimensional morphometric analysis of human cancellous bone: microstructural data from spine, femur, iliac crest, and calcaneus. J Bone Miner Res, 1999. **14**(7): p. 1167-74.
26. Hulme, P.A., S.K. Boyd, and S.J. Ferguson, Regional variation in vertebral bone morphology and its contribution to vertebral fracture strength. Bone, 2007. **41**(6): p. 946-57.
27. Lochmuller, E.M., et al., Does thoracic or lumbar spine bone architecture predict vertebral failure strength more accurately than density? Osteoporos Int, 2008. **19**(4): p. 537-45.
28. Baroud, G., et al., Effect of vertebral shell on injection pressure and intravertebral pressure in vertebroplasty. Spine (Phila Pa 1976), 2004. **30**(1): p. 68-74.
29. Nauman, E.A., K.E. Fong, and T.M. Keaveny, Dependence of intertrabecular permeability on flow direction and anatomic site. Ann Biomed Eng, 1999. **27**(4): p. 517-24.
30. Ahn, H., et al., The effect of pre-vertebroplasty tumor ablation using laser-induced thermotherapy on biomechanical stability and cement fill in the metastatic spine. Eur Spine J, 2007. **16**(8): p. 1171-8.
31. Reidy, D., et al., A biomechanical analysis of intravertebral pressures during vertebroplasty of cadaveric spines with and without simulated metastases. Spine (Phila Pa 1976), 2003. **28**(14): p. 1534-9.
32. Krebs, J., et al., Clinical measurements of cement injection pressure during vertebroplasty. Spine (Phila Pa 1976), 2005. **30**(5): p. E118-22.
33. Anselmetti, G.C., et al., Percutaneous vertebroplasty and bone cement leakage: clinical experience with a new high-viscosity bone cement and delivery system for vertebral augmentation in benign and malignant compression fractures. Cardiovasc Intervent Radiol, 2008. **31**(5): p. 937-47.
34. Barragan-Campos, H.M., et al., Percutaneous vertebroplasty for spinal metastases: complications. Radiology, 2006. **238**(1): p. 354-62.
35. Calmels, V., et al., Osteoblastic and mixed spinal metastases: evaluation of the analgesic efficacy of percutaneous vertebroplasty. AJNR Am J Neuroradiol, 2007. **28**(3): p. 570-4.
36. Tseng, Y.Y., et al., Percutaneous polymethylmethacrylate vertebroplasty in the treatment of pain induced by metastatic spine tumor. Surg Neurol, 2008. **70 Suppl 1**: p. S1:78-83; discussion S1:83-4.
37. Yang, Z., et al., Treatment of metastatic spinal tumors by percutaneous vertebroplasty versus percutaneous vertebroplasty combined with interstitial implantation of 125I seeds. Acta Radiol, 2009. **50**(10): p. 1142-8.

38. Lador, R., et al., A pictorial classification atlas of cement extravasation with vertebral augmentation. Spine J, 2010. **10**(12): p. 1118-27.
39. Gosev, I., et al., Right ventricular perforation and pulmonary embolism with polymethylmethacrylate cement after percutaneous kyphoplasty. Circulation, 2013. **127**(11): p. 1251-3.
40. Habib, N., et al., Cement pulmonary embolism after percutaneous vertebroplasty and kyphoplasty: an overview. Heart Lung, 2012. **41**(5): p. 509-11.
41. Tourtier, J.-P. and S. Cottez, Pulmonary Cement Embolism after Vertebroplasty. New England Journal of Medicine, 2012. **366**(3): p. 258-258.
42. Sidhu, G.S., et al., Neurological deficit due to cement extravasation following a vertebral augmentation procedure. J Neurosurg Spine, 2013. **19**(1): p. 61-70.
43. Liebschner, M.A., W.S. Rosenberg, and T.M. Keaveny, Effects of bone cement volume and distribution on vertebral stiffness after vertebroplasty. Spine (Phila Pa 1976), 2001. **26**(14): p. 1547-54.
44. Tschirhart, C.E., S.E. Roth, and C.M. Whyne, Biomechanical assessment of stability in the metastatic spine following percutaneous vertebroplasty: effects of cement distribution patterns and volume. Journal of Biomechanics, 2005. **38**(8): p. 1582-1590.

**Table 1.** The location and size of all elements incorporated into the 3D bone surrogates. All coordinates are measured with respect to the geometrical centre of each element.

| Surrogate | Element | Coordinate | | | Description |
|---|---|---|---|---|---|
| | | x | y | z | |
| Osteo, Lesion and MM | 1 | 0.0 | 0.0 | 0.0 | Reference point |
| | 2 | 20.0 | 0.0 | 15.3 | Outlet, circular Ø 3.0 mm |
| | 3 | 13.5 | -20.6 | 8.0 | Inlet, circular Ø 2.1 mm |
| | 4 | 8.2 | -26.1 | 9.3 | Outlet, elliptical width 1.0 and height 2.0 mm |
| | 5 | 31.8 | -26.1 | 9.3 | Outlet, elliptical width 1.0 and height 2.0 mm |
| Lesion | 6 | 14.3 | 0.0 | 10.0 | Outlet, circular Ø 2.7 mm |
| | 7 | 14.3 | -8.9 | 10.0 | Spherical void Ø 19.0 mm |
| MM | 6 | 14.3 | 0.0 | 8.0 | Outlet, circular Ø 2.6 mm |
| | 7 | 14.3 | -2.2 | 8.0 | Spherical void Ø 6.0 mm |
| | 8 | 14.3 | -14.9 | 8.0 | Spherical void Ø 6.0 mm |
| | 9 | 14.3 | -23.4 | 8.0 | Spherical void Ø 6.0 mm |

**Figure 1**

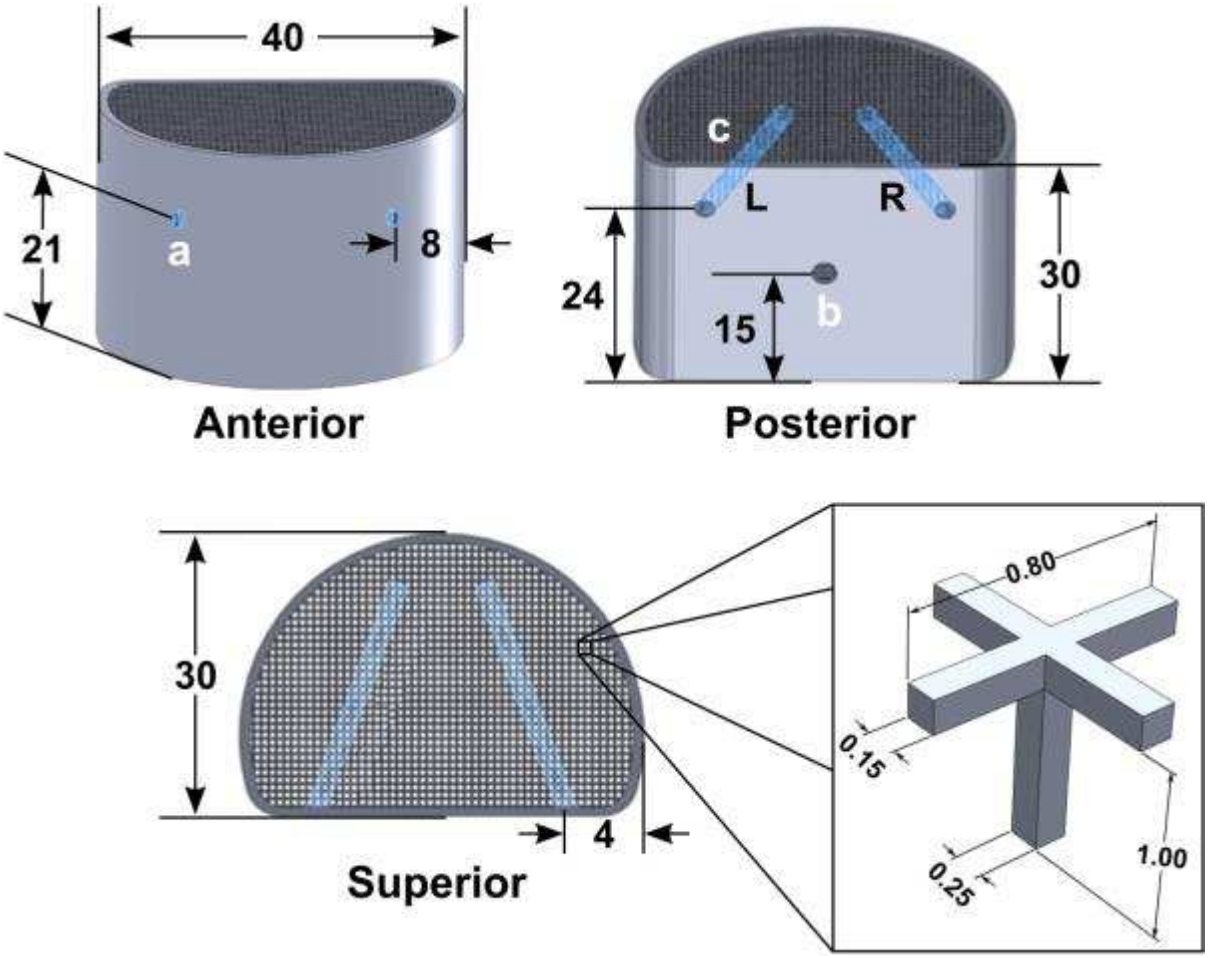
40
21
a
8
Anterior
c
L
R
24
15
b
30
Posterior
30
4
Superior
0.80
0.15
0.25
1.00

**Figure 2**

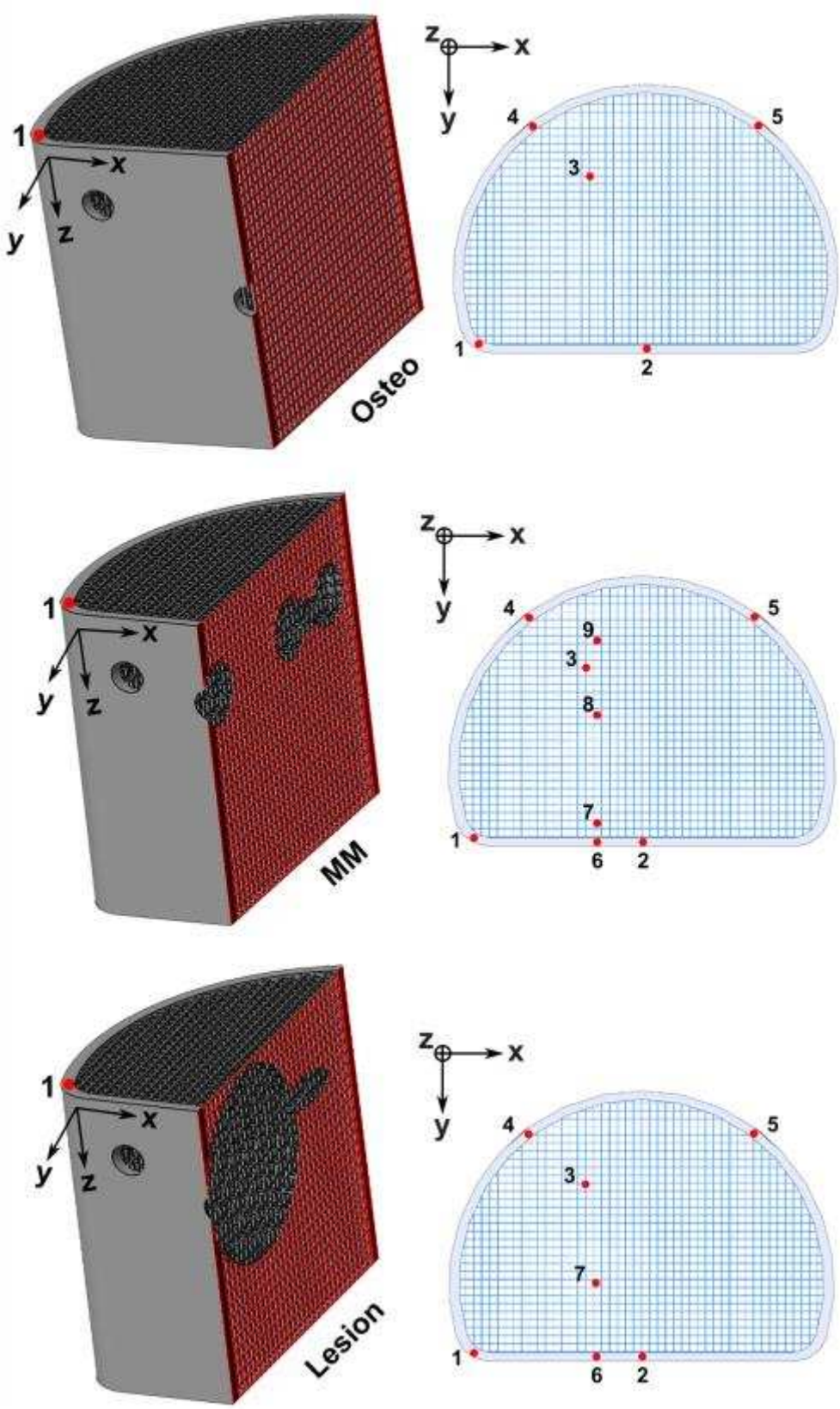

**Figure 3**

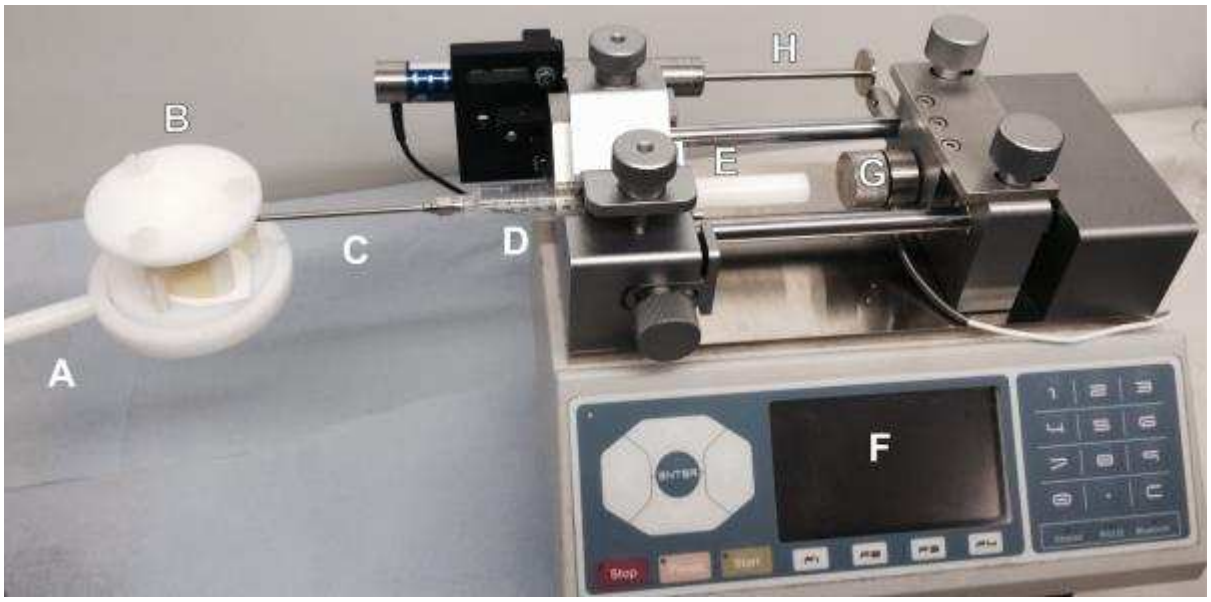

**Figure 4**

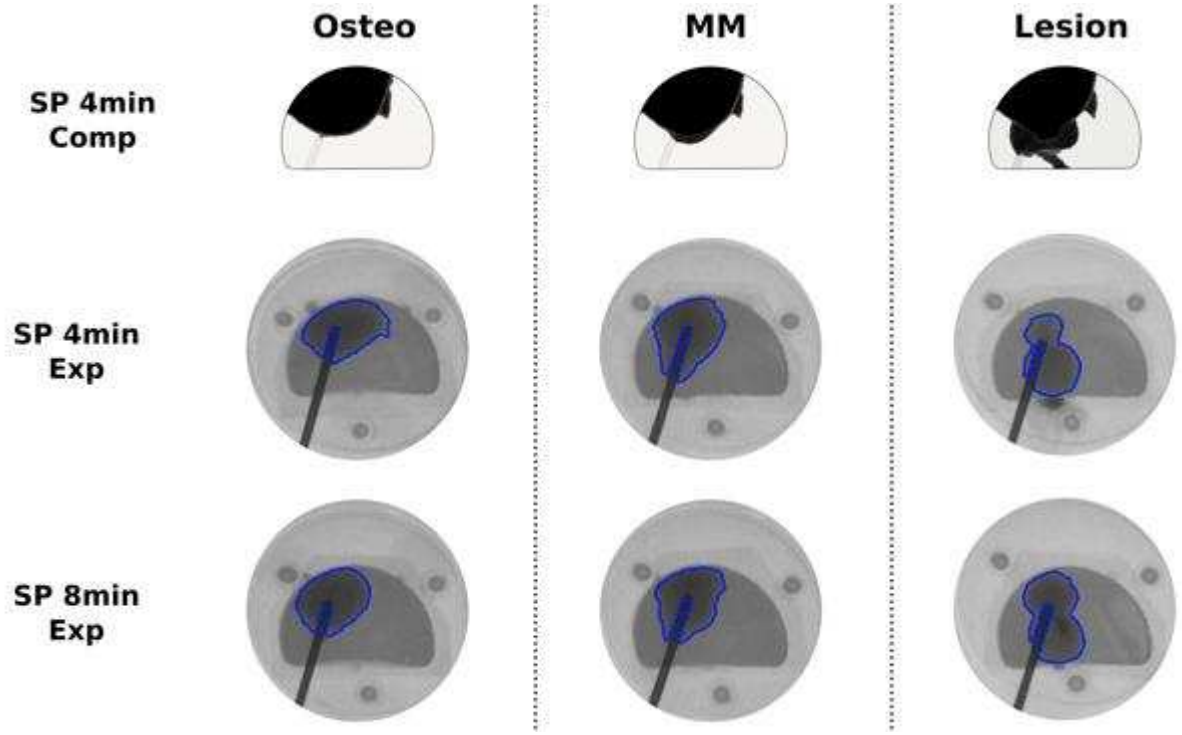

**Figure 5**

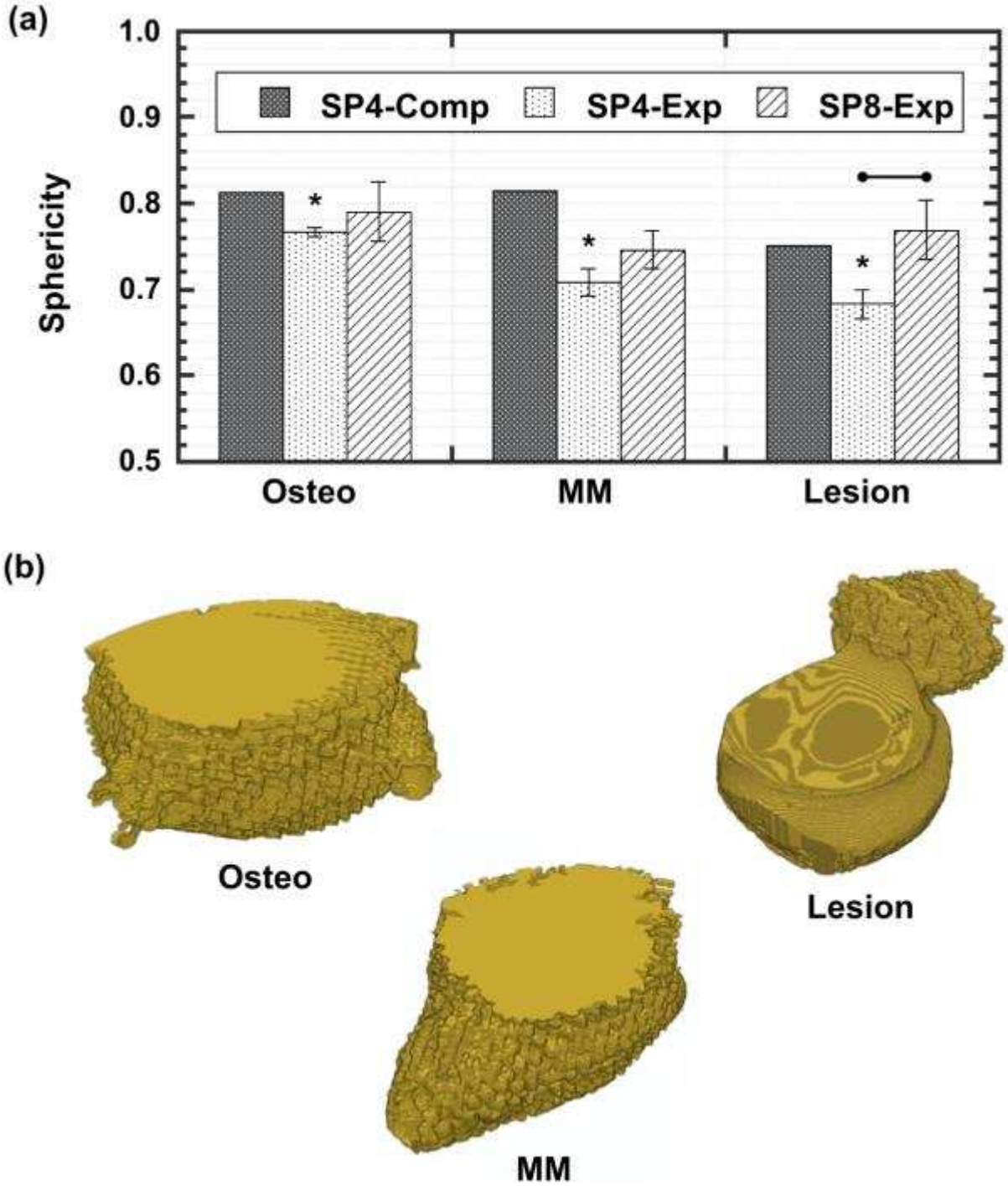
(a)
1.0
0.9
0.8
0.7
0.6
0.5
Sphericity
SP4-Comp
SP4-Exp
SP8-Exp
*
*
*
Osteo
MM
Lesion
(b)
Osteo
MM
Lesion

**Figure 6**

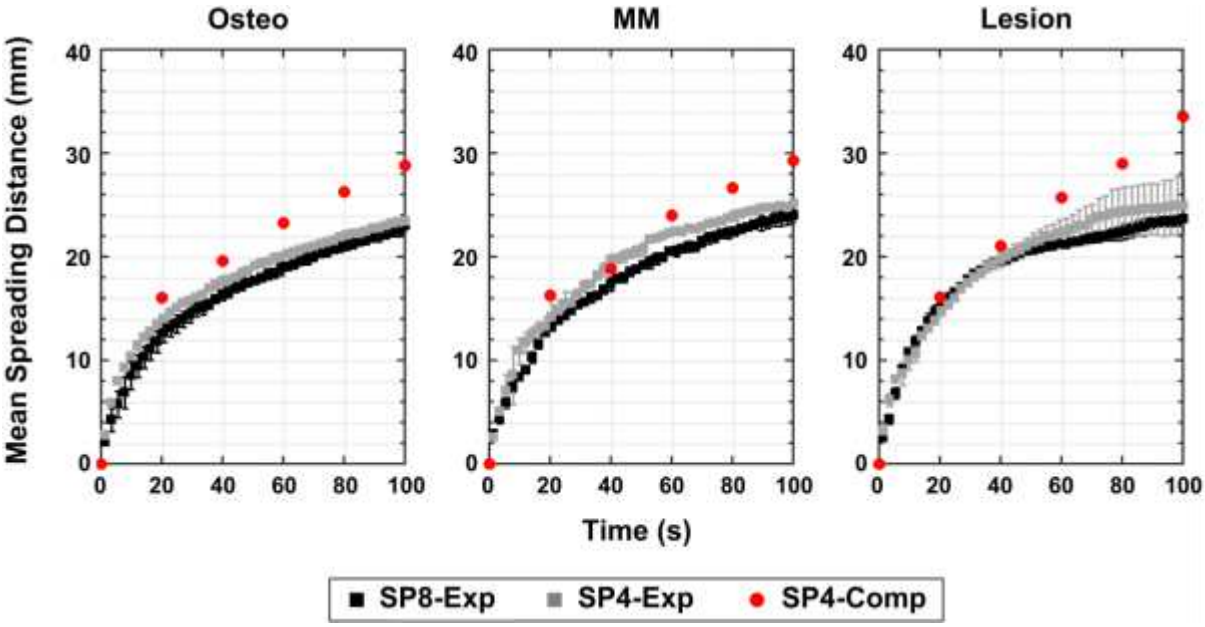
Osteo
MM
Lesion
Mean Spreading Distance (mm)
Time (s)
SP8-Exp
SP4-Exp
SP4-Comp

**Figure 7**

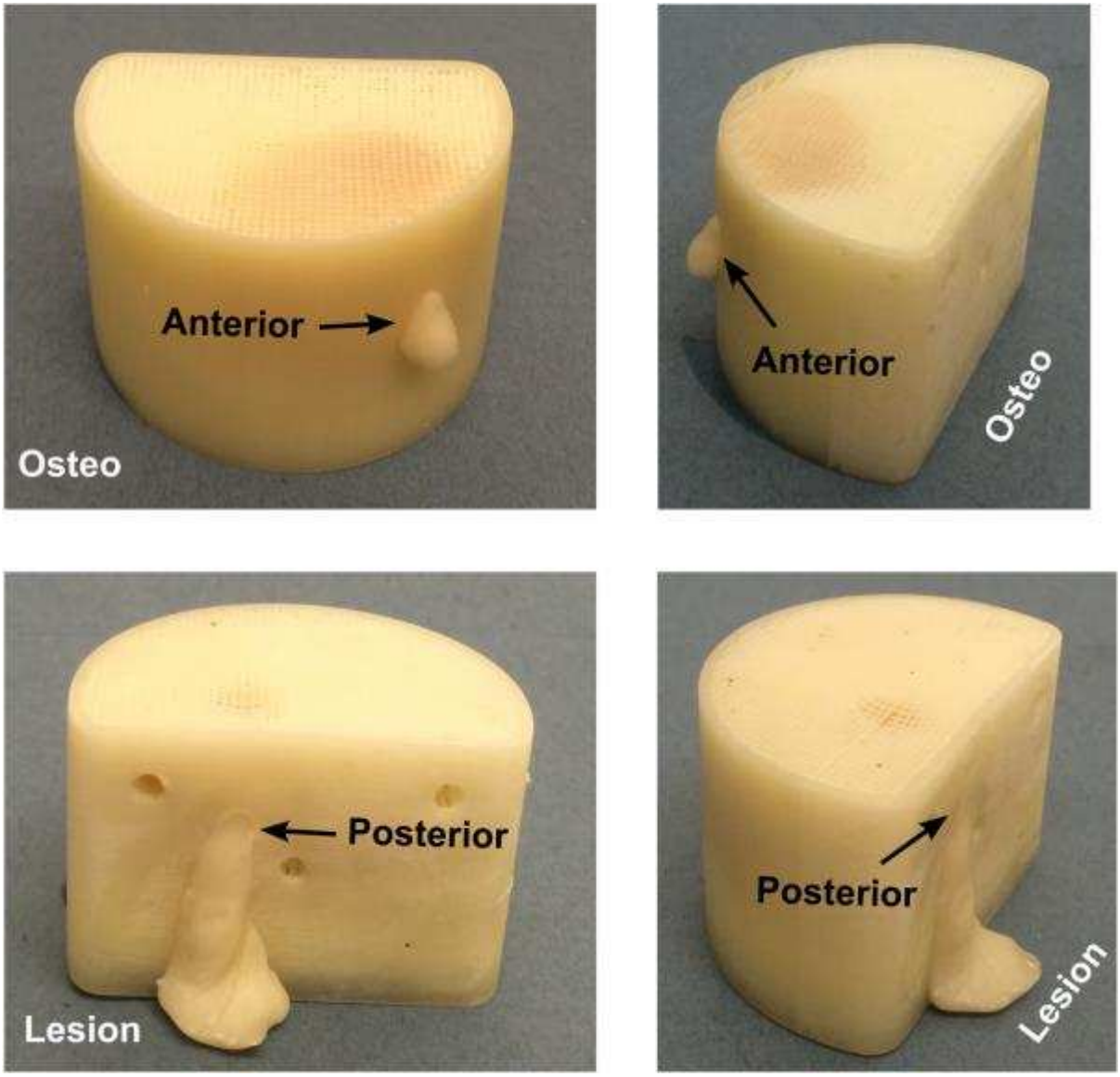
Anterior
Osteo
Anterior
Osteo
Posterior
Lesion
Posterior
Lesion

**Figure 8**

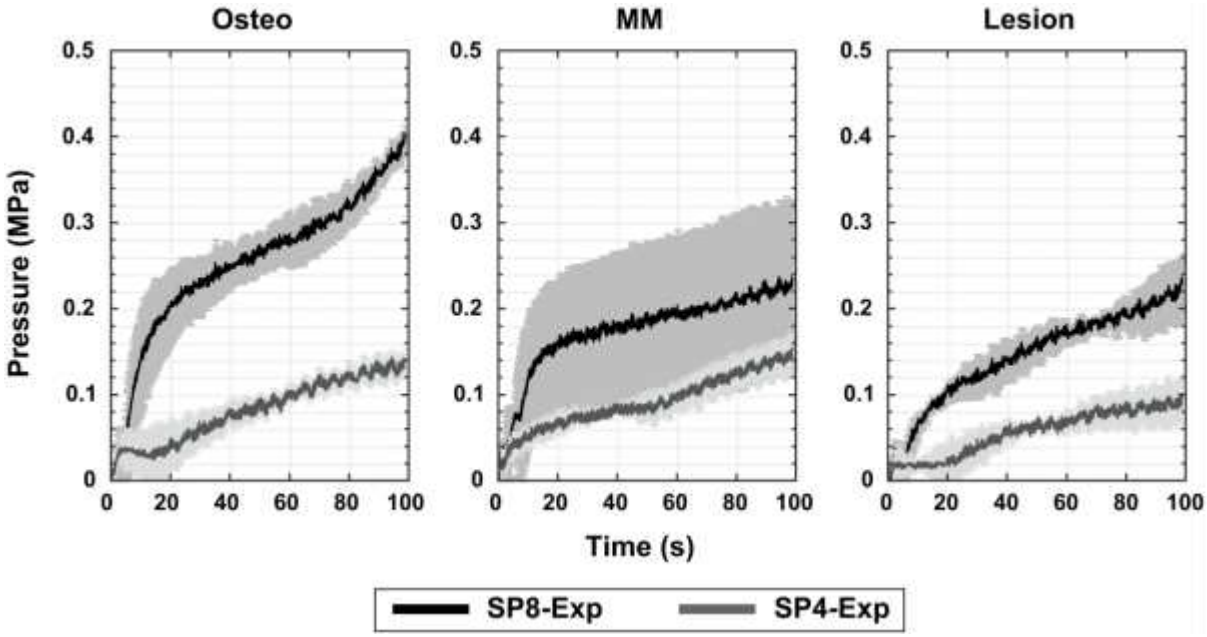
Osteo
MM
Lesion
Pressure (MPa)
0.5
0.4
0.3
0.2
0.1
0
0
20
40
60
80
100
Time (s)
SP8-Exp
SP4-Exp

**Figure 1.** The boundary of the 3D bone surrogates showing: (a) two identical and symmetrical elliptical openings 2 mm in height and 1 mm in width applied to mimic breaches due to anterior blood vessels, (b) one circular opening 3 mm in diameter applied to mimic posterior breaches due to the basivertebral veins, and (c) the insertion channels that were incorporated to allow consistent needle placement during injection. The superior and inferior surfaces of the surrogates were kept open due to manufacturing restrictions. All dimensions are in millimetres.

**Figure 2.** The developed 3D bone surrogates. (Left) Section-view of the Osteo, Lesion and MM surrogates. (Right) Craniocaudal view showing the location of all elements incorporated into each surrogate (refer to Table 1).

**Figure 3.** Photograph of the experimental set-up showing: (A) the specimen holder with (B) the 3D bone surrogate, (C) the 12 gauge needle, (D) the 10 mL luer-lok syringe with (E) a custom built plastic plunger (Delrin®, DuPont, Delaware, USA), (F) the syringe pump, (G) the load cell and (H) the LVDT.

**Figure 4.** Representative images of typical flow patterns after 5mL of Simplex P cement was separately injected at 4 and 8 min after mixing (SP4 and SP8) into each 3D bone surrogate. The solid line surrounding the contours is the outline of the image segmentation performed in Matlab. The simulated flow distribution is included for comparison.

**Figure 5.** (a) The sphericity after 5 mL of Simplex P cement was separately injected at 4 and 8 min after cement mixing (SP4 and SP8) into each 3D bone surrogate at a constant flow rate of 3 mL/min. The sphericity obtained numerically for SP4 is included for comparison. The experimental data is presented as mean ± SD and the significant differences ($p < 0.05$)

are labelled * and ●—●. (b) Representative images of the SP4 cement bolus obtained from the experiments after 5 mL was injected into each 3D bone surrogate. The flat surface of the cement bolus in the Osteo and MM surrogates indicates that the cement had reached the superior plate of the specimen holder.

**Figure 6.** The mean spreading distance as a function of time after Simplex P cement was separately injected at 4 and 8 min after mixing (SP4 and SP8) into each 3D bone surrogate at a constant flow rate of 3 mL/min. The spreading distance obtained numerically for SP4 is included for comparison. The experimental data is presented as mean ± SD.

**Figure 7.** Photographs of the Osteo and Lesion surrogates showing the typical leakage observed after 5 mL of Simplex P cement was injected.

**Figure 8.** The inlet pressure as a function of time after Simplex P cement was separately injected at 4 and 8 min after mixing (SP4 and SP8) into each 3D bone surrogate at a constant flow rate of 3 mL/min. The pressure obtained numerically for SP4 is included for comparison. The experimental data is presented as mean ± SD.